Original Article: Laboratory Investigation

Glypican-1 as a target for fluorescence molecular imaging of bladder cancer

Dmitry M Polikarpov,[1] Douglas H Campbell,[2] Alexander B Zaslavsky,[3] Maria E Lund,[2] Angela Wu,[2] Yanling Lu,[2] Ganesh S Palapattu,[3] Bradley J Walsh,[2] Andrei V Zvyagin[4,5] and David A Gillatt[1]

[1]Department of Clinical Medicine, Faculty of Medicine and Health Sciences, Macquarie University, [2]GlyTherix, Sydney, New South Wales, Australia, [3]Department of Urology, University of Michigan, Ann Arbor, Michigan, USA, [4]ARC Center of Excellence for Nanoscale BioPhotonics, Macquarie University, Sydney, New South Wales, Australia, and [5]Institute of Molecular Medicine, Sechenov University, Moscow, Russia

Abbreviations & Acronyms
GPC-1 = glypican-1
IgG = immunoglobulin G
MFI = mean fluorescence intensity
NHS = *N*-hydroxy-succinimide
NIR = near-infrared
PBS = phosphate-buffered saline
PCR = polymerase chain reaction
SEC-HPLC = size exclusion chromatography high performance liquid chromatography
SEM = standard error of the mean
TBR = tumor-to-background ratio
UC = urothelial carcinoma

Correspondence: Dmitry M Polikarpov M.D., M.Res., Ph.D., Department of Clinical Medicine, Faculty of Medicine and Health Sciences, Level 1, 75 Talavera Road, Macquarie University, Sydney, NSW 2109, Australia. Email: dmitry.polikarpov@hdr.mq.edu.au

Objectives: To investigate whether anti-glypican-1 antibody Miltuximab conjugated with near-infrared dye IRDye800CW can be used for *in vivo* fluorescence imaging of urothelial carcinoma.

Methods: The conjugate, Miltuximab-IRDye800CW, was produced and characterized by size exclusion chromatography and flow cytometry with glypican-1-expressing cells. Balb/c nude mice bearing subcutaneous urothelial carcinoma xenografts were intravenously injected with Miltuximab-IRDye800CW or control IgG-IRDye800CW and imaged daily by fluorescence imaging. After 10 days, tumors and major organs were collected for *ex vivo* study of the conjugate biodistribution, including its accumulation in the tumor.

Results: The intravenous injection of Miltuximab-IRDye800CW to tumor-bearing mice showed its specific accumulation in the tumors with the tumor-to-background ratio of 12.7 ± 2.4, which was significantly higher than that in the control group (4.6 ± 0.9, $P < 0.005$). The *ex vivo* imaging was consistent with the *in vivo* findings, with tumors from the mice injected with Miltuximab-IRDye800CW being significantly brighter than the organs or the control tumors.

Conclusions: The highly specific accumulation and retention of Miltuximab-IRDye800CW in glypican-1-expressing tumors *in vivo* shows its high potential for fluorescence imaging of urothelial carcinoma and warrants its further investigation toward clinical translation.

Key words: fluorescence-guided surgery, glypican-1, molecular imaging, monoclonal antibodies, urinary bladder neoplasms.

Introduction

Approximately 75% of bladder cancer patients present with non-muscle-invasive UC with tumors confined to the urothelium and subepithelial layer.[1] Such tumors are usually removed by transurethral endoscopic resection followed by intravesical immunotherapy or chemotherapy and regular surveillance cystoscopies.[2] Although this treatment is often effective, up to 50% of patients eventually suffer recurrence or invasive progression, which might require cystectomy and systemic therapy.[3] The high rate of recurrence and long-term surveillance make bladder cancer a major health issue and economic burden.[4] An incomplete initial resection has been hypothesized to contribute to the high rates of recurrence and progression of UC.[5–7]

Fluorescence cystoscopy, using hexaminolevulinate to improve the completeness of initial resection, is one recommended option; however, it suffers from low specificity, limited contrast and the need for intravesical instillation of the drug 1–2 h before cystoscopy, with retention of the drug until the procedure.[2] Orally administered 5-ALA solves the problem of intravesical instillation; however, it shares the other shortfalls of hexaminolevulinate, including the need for careful timing between the administration and cystoscopy.[8] NIR fluorescent molecular imaging has the potential to overcome the limitations of hexaminolevulinate.[9] Such imaging usually involves the use of a conjugate of a monoclonal antibody with a NIR fluorescent dye, where the antibody and the dye provide optimal specificity and imaging

performance, respectively.[9,10] Provided the imaging antibody-dye conjugate is safe and specific, it can be administered intravenously, eliminating the need for intravesical administration and retention of the drug before cystoscopy. The intravenous administration of an antibody-dye conjugates for fluorescence-guided surgery has been studied extensively, and successfully used in clinical trials in breast and brain cancer patients.[11–14]

Recently introduced NIR dye IRDye800CW (IR800) appears to be one of the most promising candidates for intraoperative molecular imaging.[13] Although several anti-epidermal growth factor receptor monoclonal antibodies coupled to IR800 have been successfully validated in clinical trials,[11–14] the notoriously high antigenic heterogeneity of UC requires expansion of the existing suite of antibodies specific to this disease for highly sensitive and specific imaging.[15] GPC-1 is a novel oncotarget, detected in UC and a range of other solid tumors, but not in normal adult tissue.[16–23] We hypothesized that clinical stage anti-GPC-1 antibody Miltuximab, conjugated with IR800, might be suitable for fluorescence molecular imaging of UC.[24] In the present study, we report the evaluation of Miltuximab-IR800 for fluorescent molecular imaging of UC in a mouse xenograft model after its intravenous administration.

Methods

Cell lines

UC cell lines were cultured in a 5% CO_2 tissue culture incubator at 37°C following standard protocols in recommended media supplemented with 10% heat inactivated (56°C, 30 min) fetal bovine serum (Scientifix, Clayton, VIC, Australia). For subculturing, the cells were detached by incubation for 20 min in 2 mmol/L ethylenediaminetetraacetic acid in PBS at 37°C after a wash with 1× PBS.

Characterization of GPC-1 expression in UC

Analysis of the GPC-1 expression in published microarray datasets was carried out using the Oncomine (www.oncomine.org) concept analysis tool.[25] GPC-1 expression at the RNA level was analyzed in UC cell lines (T24, RT4, UM-UC-3, UM-UC-6, UM-UC-13, UM-UC-14, UM-UC-9, 5637, 253J, J82, UM-UC-10, UM-UC-12) and established patient-derived cells (**BC8149 and **BC8447). Cultured cells were lysed in Trizol (Life Technologies, Waltham, MA, USA). RNA extraction from Trizol was carried out according to the manufacturer's protocol; BioRad iScript cDNA synthesis kit was used for reverse transcriptase PCR (BioRad, Hercules, CA, USA). RNA from BC8149 and BC8447 was kindly provided by Dr Philip Palmbos (UM). Quantitative PCR was carried out using BioRAD SYBR Green Mastermix on an Applied Biosystems 7300 Real-Time PCR system. All reactions were carried out in triplicates. Fold mRNA expression was calculated using the $2^{-\Delta\Delta CT}$ method.[26] Human GPC-1 primers were purchased from Sino Biological (Cat # HP100583; Beijing, China).

At the protein level, we characterized the GPC-1 expression in UC by immunohistochemistry, western blot and flow cytometry. Immunohistochemistry was carried out using tissue microarrays with single cores of 51 UC from the University of Michigan Rogel Cancer Center Tissue and Molecular Pathology Core. Staining for GPC-1 was carried out on an autostainer (Dako, Glostrup, Denmark). Stained slides were interpreted as positive when >5% of tumor cells showed strong reactivity with the antibody. Western blot was carried out as previously described.[27] The quantification of GPC-1 in UC cells was carried out by flow cytometry using anti-GPC-1 antibody MIL-38 (GlyTherix, Sydney, NSW, Australia), a murine version of Miltuximab and a QIFIKIT (Quantitative Immunofluorescence Intensity kit; Dako) following the manufacturer's protocol.

Conjugation of Miltuximab with IR800 and its characterization

Miltuximab (GlyTherix) was conjugated with the NHS ester of the NIR fluorescent dye IR800 (for lysine binding on the antibody) using an IRDye 800CW Protein Labeling Kit – High MW (928-33040; Li-Cor Biosciences, Lincoln, NE, USA) as per the manufacturer's protocol. The Miltuximab-IR800 conjugate was subsequently separated from free dye using a centrifugal column. To determine the final concentration of the conjugate and the dye/antibody molar ratio, absorbance spectra at 280 nm and 780 nm were determined by a microplate reader Pherastar (BMG Labtech, Ortenberg, Germany). As a control, a human IgG isotype control antibody (cat # 31154; Thermo Fisher Scientific, Waltham, MA, USA) was conjugated with IR800 and characterized using the same method. The purities of the antibody and conjugates were analyzed by SEC-HPLC on an Agilent Bio SEC-3 column with UV detection at 280 nm, flow rate of 0.3 mL/min and column temperature of 25°C. A control protein standard mixture (Bio-Rad) was run before analysis of each sample. The binding of Miltuximab-IR800 to UC-6 cells *in vitro* was compared with that of unconjugated Miltuximab and control IgG-IR800 with the same cell line by flow cytometry following previously published protocol.[20]

Establishment of subcutaneous xenografts

The work with animals was carried out in accordance with the Australian code for the care and use of animals for scientific purposes, and approved by Macquarie University Animal Ethics Committee (AEC Reference No.: 2018/015). UC-6 cells in serum-free media with Matrigel Basement Membrane matrix (Corning, Corning, NY, USA) were subcutaneously inoculated to 10 8-week-old Balb/c nude female mice (Animal Resource Center, Canning Vale, WA, Australia) anesthetized by 2% isoflurane inhalation through a nose cone. The mice were monitored for signs of distress and weighed daily, while the tumor growth was monitored twice weekly by caliper measurement.

Intravenous administration of Miltuximab-IR800 and *in vivo* imaging

When the tumors reached 1000 mm^3 in volume, eight mice with tumors of equivalent size were selected, randomized into

two groups of four and intravenously injected with 6 mg/kg of Miltuximab-IR800 or the control IgG-IR800. For the injection, the mice were illuminated by a heating lamp for 10 min and anesthetized by 5% isoflurane inhalation through a nose cone. The injection was then given into the tail vein using a 1-mL syringe with a 30-G needle, followed by supervised recovery.

After the intravenous administration of the conjugate, the mice were monitored daily for signs of toxicity and imaged daily by a fluorescence imager Odyssey CLx (Li-Cor Biosciences) at 3 h, 10 h and 24 h post-injection, and then daily for 10 days. The imaging was carried out using Image Studio software (Li-Cor Biosciences). Regions of interest of equal size were placed on the tumor and on the mouse back away from the tumor. The total fluorescence intensity of these regions was then used to calculate the TBR.

Ex vivo study of the biodistribution of Miltuximab-IR800

A total of 10 days after the conjugate administration, the tumor and major organs were collected from the mice and imaged by the Odyssey CLx imager. To assess the distribution of the conjugate within the tumor, 5-μm sections were prepared and studied by the Odyssey CLx imager. By using Image Studio software, each organ or tumor section was selected as a region of interest and the MFI of these regions was compared.

Statistical analysis

The values are expressed as the mean $\pm$ SEM. The statistical analyses were carried out using GraphPad Prism 8.3.0 software (GraphPad Software, San Diego, CA, USA). The *in vivo* TBR and *ex vivo* MFI were compared between the groups using the unpaired Student's *t*-test with Welch's correction. A *P*-value of <0.05 was considered statistically significant.

Results

GPC-1 expression in UC

We confirmed GPC-1 overexpression in infiltrating UC at the RNA level using a public database (Oncomine; Fig. 1a), and quantitative PCR carried out on cell lines and patient-derived cells (Fig. 1b). The GPC-1 overexpression at the protein level was confirmed by positive immunohistochemical staining in high-grade invasive UC tissue samples from a tissue microarray (Fig. 1c) and by western blot in UC cell lines 5637, UC-14, UC-9, UC-6, UC-13, UC-3 and high-grade infiltrating patient-derived UC cells (**BC8149 and **BC8447) using prostate cancer cell lines LNCaP and DU-145 as a negative and positive controls, respectively (Fig. 1d). Additionally, we carried out the flow cytometry assaying and quantified the expression of GPC-1 in UC cell lines T-24 and UC-6 (Fig. S1).

Characterization of Miltuximab-IR800

An NHS ester of the NIR fluorescent dye IR800 was conjugated with Miltuximab or a control isotype human IgG_1 antibody. The final concentration was found to be 0.57 mg/mL, and the average dye-to-protein molecular ratio was approximately 1:1 in both conjugates. Miltuximab-IR800 was subsequently characterized by SEC-HPLC and compared with unconjugated Miltuximab. The Miltuximab-IR800 was found to be $81.3 \pm 1.3\%$ monomeric, which was lower than $90.2 \pm 0.1\%$ for unconjugated Miltuximab. Such reduction of the monomeric fraction is consistent with approximately 90% of Miltuximab molecules being labeled by IR800. SEC-HPLC has also shown an increase in the retention time of the conjugate, in line with an increase of molecular weight.

The flow cytometry analysis confirmed that the conjugation did not affect the binding of Miltuximab-IR800 to UC cells
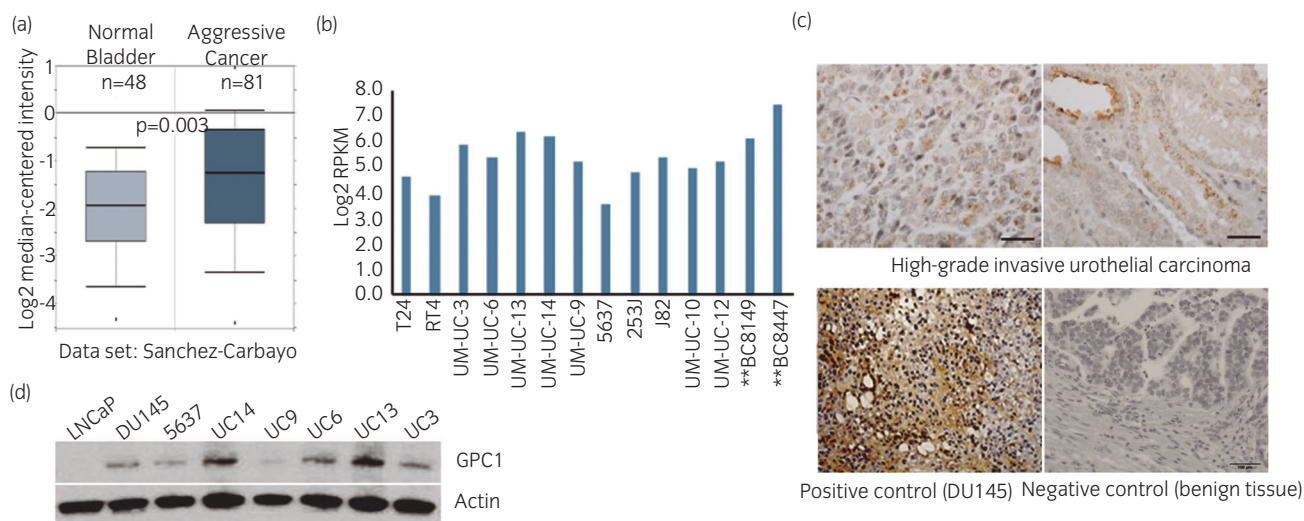

Fig. 1 Expression of GPC-1 in UC tissues, cell lines and tissue microarrays. (a) cDNA microarray data analysis from public database (Oncomine) confirmed GPC-1 overexpression in samples from patients with UC. (b) qPCR was carried out for GPC-1 expression in a panel of UC cell lines and established patient-derived cells (**BC8149 and **BC8447). (c) Immunohistochemical staining of GPC-1 of UC tissue microarray sections. (d) GPC-1 protein expression in UC cell lines analyzed by western blot with prostate cancer cell lines LNCaP and DU-145 as negative and positive controls, respectively, and actin as a loading control.
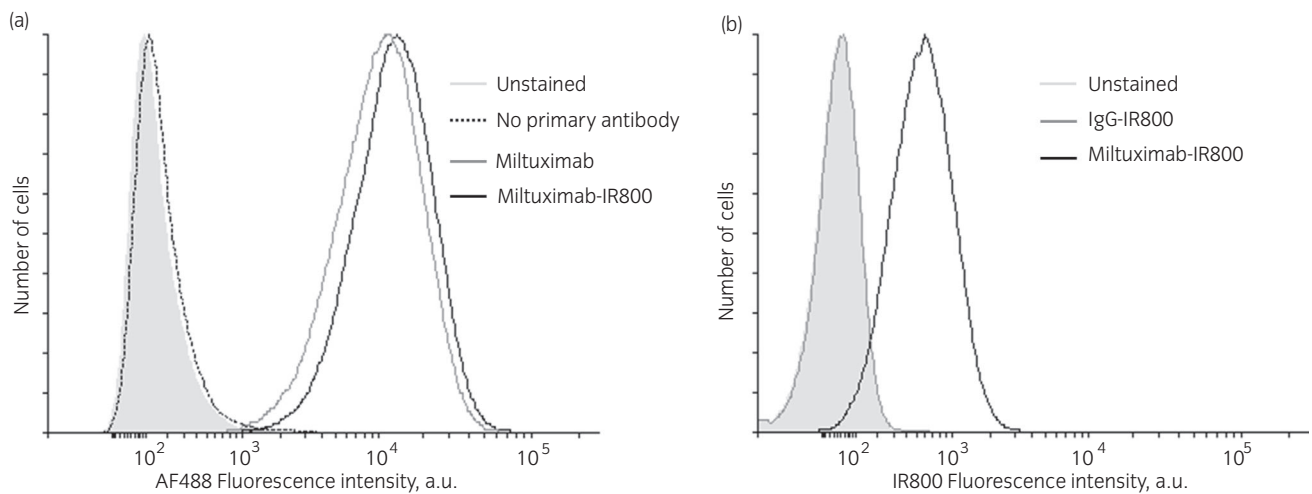
Fig. 2 Flow cytometry analysis of the binding of Miltuximab-IR800 to UC-6 cells compared with (a) unconjugated Miltuximab or (b) IgG-IR800. (a) The light grey filled histogram represents unstained cells, dashed black line shows the cells incubated only with secondary antibody, solid grey line shows the cells incubated with unconjugated Miltuximab and solid black line shows the cells labeled by Miltuximab-IR800. (b) The light grey filled histogram represents unstained cells, solid grey line shows the cells incubated with IgG-IR800 and solid black line shows the cells labelled by Miltuximab-IR800.

UC-6 (98.93 ± 1.33% positive; MFI = 12 273 ± 622 a.u.), which was not significantly different from that of unconjugated Miltuximab (99.83 ± 0.08% positive; MFI = 10 166 ± 2726 a.u.; Fig. 2a). As shown in Figure 2b, flow cytometry also confirmed NIR fluorescence of Miltuximab-IR800 (MFI = 543.3 ± 11.9 a.u.) and lack of binding of the control conjugate IgG-IR800 to UC-6 cells (MFI = 23.0 ± 0.6 a.u.).

In vivo fluorescence imaging

To assess the specific tumor accumulation of Miltuximab-IR800, we prepared a group of eight mice inoculated with UC-6 cells on the hind limb. The group was split into four tested and four control animals, and intravenously injected with Miltuximab-IR800 or IgG-IR800 as a control for passive accumulation. The mice were imaged *in vivo* at 3 h, 24 h and then daily for 10 days using a fluorescence imager (Fig. 3a,b). As shown in Figure 3b, the TBR (contrast) showed persistent growth over the observation period. Although the TBR was comparable between the groups on day 1 (Miltuximab-IR800 TBR = 2.2 ± 0.23; IgG-IR800 TBR = 1.9 ± 0.16), by day 10, the decreasing background fluorescence (Fig. 3c,d) resulted in the contrast increase. This trend was especially prominent in the animals administered with Miltuximab-IR800. TBR of this group reached 12.7 ± 2.35 and was significantly greater than that of the control group (4.6 ± 0.91, $P < 0.005$).

Biodistribution of systemically administered Miltuximab-IR800

The laboratory animals were killed on day 10 after the injection of Miltuximab-IR800, and their tumors and major organs were collected for *ex vivo* fluorescence imaging. Panels (a) and (b) of Figure 4 show that the tumors of the mice injected with Miltuximab-IR800 exhibited greater uptake of IR800 measured in terms of the fluorescence intensity,

MFI = 1082 ± 298 a.u. MFI in the tumors was greater than that in the organs (MFI = 159 ± 71 a.u.) or tumors extracted from the control mice (MFI = 540 ± 113 a.u.). Injection of Miltuximab-IR800 resulted in a higher tumor-to-liver ratio than that of the control group (6.0 ± 1.3 *vs* 2.2 ± 0.1, respectively). This result speaks in favor of the specificity of the tumor targeting by Miltuximab-IR800. Also, in line with the specific accumulation of Miltuximab-IR800 in the tumor and less unbound conjugate in circulation, the fluorescence of the skin, spleen and heart was lower in these mice compared with the control group.

The tumors were subsequently sectioned and re-imaged to avoid artefacts of whole-organ imaging and better assess the sensitivity of the imaging with Miltuximab-IR800. Panels (c) and (d) of Figure 4 show that 5-μm tumor sections from the mice injected with Miltuximab-IR800 produced approximately twofold stronger fluorescence (MFI = 52.1 ± 9.7 a.u.) than that of the tumor sections of the same thickness from the control mice (MFI = 23.7 ± 6.1 a.u.). These findings were consistent with the assessment of the specific and non-specific tumor uptake in the whole-mouse *in vivo* and whole-organ *ex vivo* imaging, and support specific accumulation of Miltuximab-IR800 in the tumor.

Discussion

We investigated the application of fluorescent immunoconjugate, Miltuximab-IR800, for molecular imaging of UC. First, we confirmed overexpression of GPC-1 in UC, but not normal urothelium, on genetic and protein levels using genetic database, cell lines and tissue microarrays. We then conjugated Miltuximab with IR800 and confirmed that its binding to GPC-1-expressing cells is comparable to that of unconjugated Miltuximab. The accumulation of Miltuximab-IR800 in tumors *in vivo* was established using subcutaneous UC xenografts and systemic administration of the tested immunoconjugate. We found that Miltuximab-IR800 was successfully
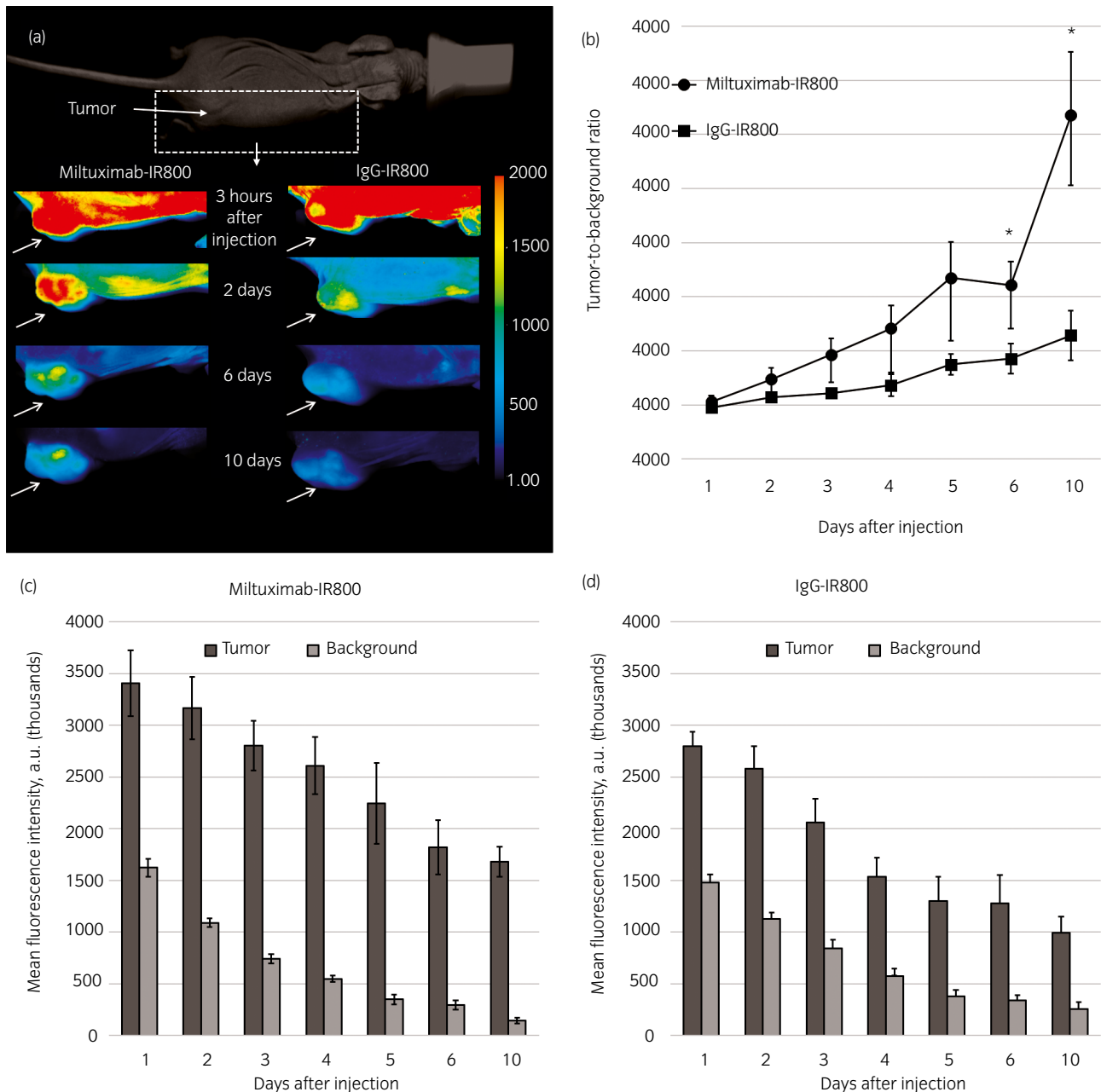
Fig. 3 Imaging and analysis of *in vivo* biodistribution of Miltuximab-IR800 or IgG-IR800 in tumor-bearing and control mice. (a) Representative false-color images of the mice injected with Miltuximab-IR800 or IgG-IR800 at 3 h, 2, 6 and 10 days after intravenous injection with constant imaging parameters and minimum/maximum pixel values. White arrow points at the tumor. (b) Line graph showing tumor-to-background ratio in mice injected with Miltuximab-IR800 or IgG-IR800. (c,d) Bar charts showing the total fluorescence intensity from the regions of interest of equal size placed on the tumor or the back of the mice injected with (c) Miltuximab-IR800 or (d) IgG-IR800. Data are the mean ± SEM, $n = 4$, *$P < 0.05$.

delivered to the tumors producing high fluorescence contrast, with contrast increasing over 10 days. The results of the *ex vivo* investigation of the animal tumors and organs corroborated the *in vivo* findings, and confirmed the specific accumulation and retention of Miltuximab-IR800 in the tumors. Bright fluorescence of 5-μm tumor sections showed high sensitivity of this technique, which is crucial for the thorough detection of the residual pathology after resection.

The high specificity of Miltuximab-IR800 was shown by the lower TBR in the mice treated with the control conjugate IgG-IR800. The low-level tumor fluorescence caused by IgG-IR800 was likely due to passive accumulation and enhanced permeability and retention effect of tumors; however, it was far inferior to that of Miltuximab-IR800.[28] Compared with the control group, the mice injected with Miltuximab-IR800 had twofold higher fluorescence of the tumor and,
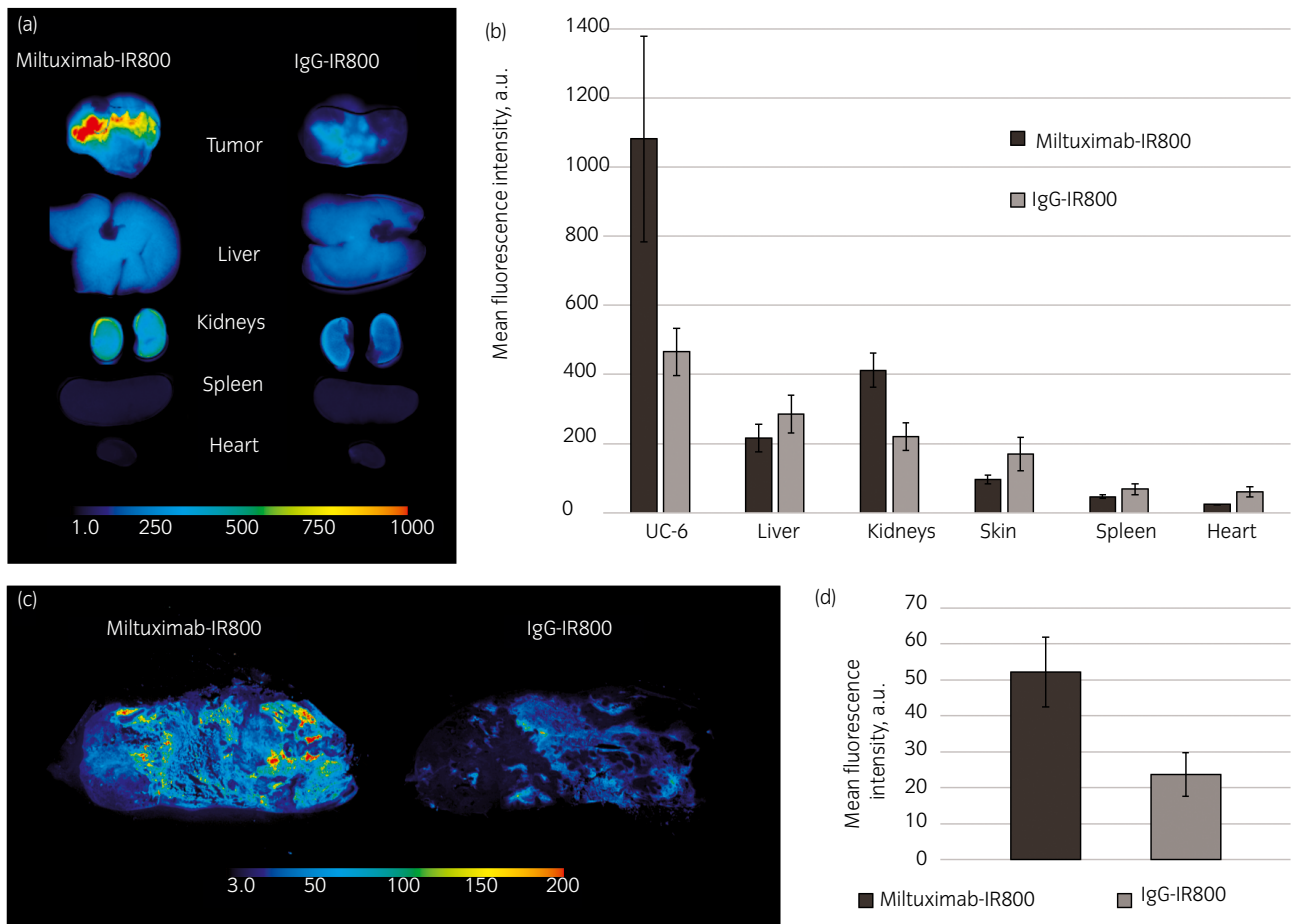
Fig. 4 *Ex vivo* assessment of the biodistribution of Miltuximab-IR800. (a) *Ex vivo* fluorescence imaging of UC-6 tumors and major organs removed from the mice on day 10 after the intravenous injection of (left) Miltuximab-IR800 or (right) IgG-IR800. (b) Fluorescence of the whole tumors and organs from *ex vivo* imaging. (c) Representative sections of the tumors removed from the mice injected with Miltuximab-IR800 (left) or IgG-IR800 (right), and (d) their fluorescence intensity,

importantly, an approximately threefold higher tumor-to-liver ratio, which further supports high specificity of the tumor accumulation of Miltuximab-IR800. Due to the washout of the unbound conjugate from normal tissue, and its retention in the tumor, the TBR reached 2.2 allowing tumor visualization as early as 24 h after the injection, and continued to grow throughout the following 10-day period, an important characteristic for an imaging agent that can be delivered days before imaging in a clinical setting. Importantly, while some heterogeneity in fluorescence can be appreciated in tumor sections due to a combination of cancer cells and connective tissue, fluorescence could be detected throughout the tumor (Fig. 4), which is critical for the detection of tumor margins during guided resection and supports the potential utility of Miltuximab-IR800 for this purpose.

A number of imaging agents have been previously developed for intravesical application. Although intravesical delivery might appear advantageous because of the reduced systemic access of drugs, it is associated with practical difficulties, such as catheterization of the bladder before the procedure and requiring the patient to retain the drug in the bladder.[29] Furthermore, recently, Pan *et al*. have identified that

intravesically instilled quantum dots entered the circulation with ensuing accumulation in other organs, potentially mediating off target effects.[29] In contrast to the previous studies, we aimed to develop a conjugate that could be administered intravenously to mitigate the need for bladder catheterization and improve access to the deeper tumor layers.[30,31]

Based on our work and existing data, Miltuximab-IR800 has a potential to aid in detection of small flat tumors and non-resected malignant tissue at tumor margins during cystoscopy. It could be administered intravenously before cystoscopy and detected by intraoperative fluorescence imaging. The next stage of our work will validate Miltuximab-IR800 in an orthotopic model of UC. It will allow us to carry out a head-to-head comparison of the intravesical and intravenous administration of Miltuximab-IR800, and elucidate its performance in accessing and marking tumor margins. Apart from the tumor imaging performance, such study would involve assessment of the differences in the biodistribution of the conjugate after systemic or topical administration. To increase the translational relevance of our future work, we intend to validate Miltuximab-IR800-assisted tumor detection by using an open-field clinical fluorescence-imaging device. In addition

to fluorescence cystoscopy, other applications of Miltuximab-IR800, such as intraoperative visualization of metastatic disease in lymph nodes and other organs, or fluorescence urine cytology, could be investigated in the future.

Although a comprehensive assessment of the safety of Miltuximab-IR800 will be critical for clinical translation, existing data on the safety of Miltuximab and IR800 antibody conjugates is excellent. In addition to the safety shown by anti-GPC-1 antibodies in mice at up to 50 mg/kg,[18] the safety of radio-labelled Miltuximab was recently shown in a clinical trial.[24] The safety of IR800 antibody conjugates has been investigated even more extensively, and shown in multiple animal models and clinical trials.[13,32–38]

In conclusion, the present study for the first time identified GPC-1 as a target for molecular imaging of UC and reported the experimental use of Miltuximab-IR800 in laboratory animals. The proof-of-concept work described herein shows excellent targeting and retention to the tumor and its high-contrast visualization when Miltuximab-IR800 is delivered intravenously. Together with existing data on Miltuximab and IR800-based immunoconjugates, the present findings highlight the potential of Miltuximab-IR800 as an agent for fluorescence molecular imaging of UC.

Acknowledgments

Conflict of interest

DHC, AW, MEL, YL and BJW are employed by GlyTherix. ABZ and GSP received grants and other funding with GlyTherix. The other authors declare no conflict of interest.

References

1 Burger M, Catto JWF, Dalbagni G *et al*. Epidemiology and risk factors of urothelial bladder cancer. *Eur. Urol.* 2013; **63**: 234–41.

2 Babjuk M, Böhle A, Burger M *et al*. EAU guidelines on non-muscle-invasive urothelial carcinoma of the bladder: update 2016. *Eur. Urol.* 2017; **71**: 447–61.

3 Solsona E, Iborra I, Dumont R, Rubio-Briones J, Casanova J, Almenar S. The 3-month clinical response to intravesical therapy as a predictive factor for progression in patients with high risk superficial bladder cancer. *J. Urol.* 2000; **164**(3 Part 1): 685–9.

4 Yeung C, Dinh T, Lee J. The health economics of bladder cancer: an updated review of the published literature. *Pharmacoeconomics* 2014; **32**: 1093–104.

5 Brauers A, Buettner R, Jakse G. Second resection and prognosis of primary high risk superficial bladder cancer: Is cystectomy often too early? *J. Urol.* 2001; **165**: 808–10.

6 Miladi M, Peyromaure M, Zerbib M, Saïghi D, Debré B. The value of a second transurethral resection in evaluating patients with bladder tumours. *Eur. Urol.* 2003; **43**: 241–5.

7 Shariat SF, Palapattu GS, Karakiewicz PI *et al*. Discrepancy between clinical and pathologic stage: impact on prognosis after radical cystectomy. *Eur. Urol.* 2007; **51**: 137–51.

8 Yamamoto S, Fukuhara H, Karashima T, Inoue K. Real-world experience with 5-aminolevulinic acid for the photodynamic diagnosis of bladder cancer: diagnostic accuracy and safety. *Photodiagnosis Photodyn. Ther.* 2020; **32**: 101999.

9 Nguyen QT, Tsien RY. Fluorescence-guided surgery with live molecular navigation-a new cutting edge. *Nat. Rev. Cancer* 2013; **13**: 653–62.

10 Vahrmeijer AL, Hutteman M, van der Vorst JR, van de Velde CJH, Frangioni JV. Image-guided cancer surgery using near-infrared fluorescence. Nature reviews. *Clin. Oncol.* 2013; **10**: 507–18.

11 Tummers WS, Miller SE, Teraphongphom NT *et al*. Intraoperative pancreatic cancer detection using tumor-specific multimodality molecular imaging. *Ann. Surg. Oncol.* 2018; **25**: 1880–8.

12 Rosenthal EL, Moore LS, Tipirneni K *et al*. Sensitivity and specificity of cetuximab-IRDye800CW to identify regional metastatic disease in head and neck cancer. *Clin. Cancer Res.* 2017; **23**: 4744–52.

13 Miller SE, Tummers WS, Teraphongphom N *et al*. First-in-human intraoperative near-infrared fluorescence imaging of glioblastoma using cetuximab-IRDye800. *J. Neuro Oncol.* 2018; **139**(1): 135–43.

14 van Keulen S, van den Berg NS, Nishio N *et al*. Rapid, non-invasive fluorescence margin assessment: optical specimen mapping in oral squamous cell carcinoma. *Oral. Oncol.* 2019; **88**: 58–65.

15 Warrick JI, Sjödahl G, Kaag M *et al*. Intratumoral heterogeneity of bladder cancer by molecular subtypes and histologic variants [Figure presented]. *Eur. Urol.* 2019; **75**: 18–22.

16 Saito T, Sugiyama K, Hama S *et al*. High expression of Glypican-1 predicts dissemination and poor prognosis in glioblastomas. *World Neurosurg.* 2017; **105**: 282–8.

17 Melo SA, Luecke LB, Kahlert C *et al*. Glypican-1 identifies cancer exosomes and detects early pancreatic cancer. *Nature* 2015; **523**: 177–82.

18 Harada E, Serada S, Fujimoto M *et al*. Glypican-1 targeted antibody-based therapy induces preclinical antitumor activity against esophageal squamous cell carcinoma. *Oncotarget* 2017; **8**: 24741–52.

19 Matsuda K, Maruyama H, Guo F *et al*. Glypican-1 Is overexpressed in human breast cancer and modulates the mitogenic effects of multiple heparin-binding growth factors in breast cancer cells. *Cancer Res.* 2001; **61**: 5562–9.

20 Truong Q, Justiniano IO, Nocon AL *et al*. Glypican-1 as a biomarker for prostate cancer: Isolation and characterization. *J. Cancer* 2016; **7**: 1002–9.

21 Aikawa T, Whipple CA, Lopez ME *et al*. Glypican-1 modulates the angiogenic and metastatic potential of human and mouse cancer cells. *J. Clin. Invest.* 2008; **118**: 89–99.

22 Lu H, Niu F, Liu F, Gao J, Sun Y, Zhao X. Elevated glypican-1 expression is associated with an unfavorable prognosis in pancreatic ductal adenocarcinoma. *Cancer Med.* 2017; **6**: 1181–91.

23 Walker KZ, Russell PJ, Kingsley EA, Philips J, Raghavan D. Detection of malignant cells in voided urine from patients with bladder cancer, a novel monoclonal assay. *J. Urol.* 1989; **142**: 1578–83.

24 Campbell D, Sabanathan D, Gurney H *et al*. Outcomes of the miltuximab first in human trial and proposed study design for a phase I trial 89 Zr/ 177 Lu theranostic trial. *J. Clin. Oncol.* 2019; **37** (7_suppl): 261.

25 Rhodes DR, Kalyana-Sundaram S, Mahavisno V *et al*. Oncomine 3.0: genes, pathways, and networks in a collection of 18,000 cancer gene expression profiles. *Neoplasia* 2007; **9**: 166–80.

26 Livak KJ, Schmittgen TD. Analysis of relative gene expression data using real-time quantitative PCR and the 2-ΔΔCT method. *Methods* 2001; **25**: 402–8.

27 Zaslavsky AB, Gloeckner-Kalousek A, Adams M *et al*. Platelet-synthesized testosterone in men with prostate cancer induces androgen receptor signaling. *Neoplasia* 2015; **17**: 490–6.

28 Matsumura Y, Maeda H. A new concept for macromolecular therapeutics in cancer chemotherapy: mechanism of tumoritropic accumulation of proteins and the antitumor agent smancs. *Cancer Res.* 1986; **46**(12 Part 1): 6387–92.

29 Pan Y, Chang T, Marcq G *et al*. In vivo biodistribution and toxicity of intravesical administration of quantum dots for optical molecular imaging of bladder cancer. *Sci. Rep.* 2017; **7**: 1–9.

30 Bachor R, Flotte TJ, Scholz M, Dretler S, Hasan T. Comparison of intravenous and intravesical administration of chloro- aluminum sulfonated phthalocyanine for photodynamic treatment in a rat bladder cancer model. *J. Urol.* 1992; **147**: 1404–10.

31 Bachor R, Hautmann R, Hasan T. Comparison of two routes of photosensitizer administration for photodynamic therapy of bladder cancer. *Urol. Res.* 1994; **22**: 21–3.

32 Hope CH, Deep NL, Beck LN *et al*. Use of panitumumab-irdye800 to image cutaneous head and neck cancer in mice. *Otolaryngol. Head Neck Surg.* 2013; **148**: 982–90.

33 Zinn KR, Korb M, Samuel S *et al*. IND-Directed Safety And Biodistribution Study Of Intravenously Injected Cetuximab-IRDye800 in cynomolgus macaques. *Mol. Imaging Biol.* 2015; **17**: 49–57.

34 Warram JM, de Boer E, Korb M *et al*. Fluorescence-guided resection of experimental malignant glioma using cetuximab-IRDye 800CW. *Br. J. Neurosurg.* 2015; **29**: 850–8.

35 Bhattacharyya S, Patel NL, Wei L *et al*. Synthesis and biological evaluation of panitumumab-IRDye800 conjugate as a fluorescence imaging probe for EGFR-expressing cancers. *Medchemcomm* 2014; **5**: 1337.

36 Huang R, Vider J, Kovar JL *et al*. Integrin αvβ3-targeted IRDye 800CW near-infrared imaging of glioblastoma. *Clin. Cancer Res.* 2012; **18**: 5731–40.

37 Rosenthal EL, Warram JM, de Boer E *et al*. Safety and tumor specificity of cetuximab-IRDye800 for surgical navigation in head and neck cancer. *Clin. Cancer Res.* 2015; **21**: 3658–66.

38 van Keulen S, Nishio N, Fakurnejad S *et al*. The clinical application of fluorescence-guided surgery in head and neck cancer. *J. Nucl. Med.* 2019; **60**: 758–63.

Supporting information

Additional Supporting Information may be found in the online version of this article at the publisher's web-site:

Figure S1. Histograms of the flow cytometry assays of GPC-1 expression in UC cell lines T-24 and UC-6, as well as the lymphoma cell line used as a negative control for the GPC-1 expression.